Potential Analysis of a Rear-Side Passivation for Multi-Junction Space Solar Cells based on Germanium Substrates

[1]Charlotte Weiss, [1]Jonas Schön, [1]Oliver Höhn, [1]Christian Mohr, [2]Rufi Kurstjens, [3]Bruno Boizot, [1]Stefan Janz

[1]Fraunhofer Institute for Solar Energy Systems, Freiburg, 79110, Germany; [2]Umicore Electro-optic Materials, Watertorenstraat 33, 2250 Olen, Belgium; [3]Laboratoire des Solides Irradiés, CNRS-UMR 7642, CEA- DRF-IRAMIS, Ecole Polytechnique, Université Paris-Saclay, Palaiseau Cedex, 91120, France

Abstract — **For future 4-junction Ge based multi-junction solar cells, the current generated in the Ge sub-cell gets very important. We developed an efficient rear-side passivation stack, which results in minority carrier lifetimes (τ_{eff}) ≈ 200 µs and investigated its performance in an accelerated aging experiment (1 MeV electron irradiation). The aging caused a strong lifetime decrease down to $\tau_{eff} = 4$ µs, whereas the carrier mobility stayed constant. These experimental values provide the basis for Beginning-of-Life and End-of-Life solar cell simulations, which show that the potential of the rear-side passivation for 3-junction solar-cell performance is limited, but very promising for 4-junction solar cells.**

Index Terms — **III-V solar cells – space solar cells – electron irradiation – Ge passivation – solar cell simulations**

I. INTRODUCTION

In standard 3-junction space solar cells (GaInP/GaInAs/Ge), the Ge sub-cell is not limiting the current. However, the trend goes towards 4-junction solar cells with decreasing Ge wafer thickness [1]. For both developments, a current limitation from the Ge sub-cell must be avoided. Therefore, the diffusion length of minority carriers must be increased. One possibility to solve this issue is to increase the minority carrier lifetime (τ_{eff}) by lowering the Ge doping level and passivating the Ge surface in the multi-junction cell. A good design of such a passivation layer stack can furthermore lead to a decrease of the cell temperature under operation by reflecting the sub-bandgap photons and prevent their absorption at the rear-side metal contact. A schematic for such a 3-junction cell with passivated rear side is depicted in Fig. 1.
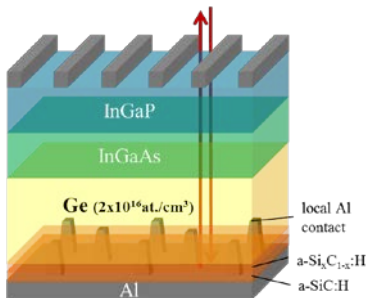

Fig. 1. Lattice-matched triple-junction solar cell with new a-Si$_x$C$_{1-x}$:H / a-SiC:H back side structure for improved reflection and excellent surface passivation including local contact points.

The Si-rich a-Si$_x$C$_{1-x}$:H layer serves as passivation layer, whereas the a-SiC:H layer leads to an enhanced reflection (indicated by the red arrows). The back contact consists of an evaporated Al layer, which is locally driven through the passivation layer stack into the Ge wafer with a laser process. For both, the enhanced reflection as well as the back contact formation a proof of concept was demonstrated earlier by Fernandez *et al.* [2, 3].

Although no significant efficiency enhancement is expected for this cell type, it represents a good reference system to investigate the effects of the new rear-side, as the manufacturing process of the 3-junction solar cell is well-established and reproducible. Later, the new back contact can easily be transmitted to 4- and 5-junction solar cell concepts.

For all space solar cells, the degradation due to irradiation with high energetic particles must be taken into account. Therefore, not only the Beginning-of-Life (BOL) but also the End-of-Life (EOL) performance has to be investigated.

In this paper we introduce a back side layer stack based on a-Si$_x$C$_{1-x}$:H for Ge surface passivation. The quality of the passivation is investigated in terms of τ_{eff} measurements by microwave detected photoconductivity decay (µW-PCD), which lead to an upper estimate of the surface recombination velocity (*S*). In a next step, we measure the lifetime decrease due to accelerated aging by 1 MeV electron irradiation. Hall measurements were conducted to prove that majority carrier mobilities (μ_{maj}) are not influenced by the electron irradiations. These results are used as input parameters for solar cell simulations in order to determine the potential of the new back-side concept for improved solar cell performance for both, BOL and EOL.

II. EXPERIMENTAL

A. Passivation

Dislocation free Czochralski 4" Ge substrates with three doping categories ("high" 9.7x10^16-1.1x10^17, "medium" 5.2-6.2x10^16, "low" ≈ 2.3x10^16 at/cm³) were provided by Umicore. The lowly doped wafers have a thickness of 500 µm, whereas the medium and highly doped wafers have a thickness of 650 µm. The removal of the oxide formed on the Ge surface was done by a dry etching step under vacuum conditions

inside a plasma enhanced chemical vapor deposition (PECVD) reactor using a H_2/Ar gas mixture for 1 min.

Fig. 2. Ge lifetime sample with a-$Si_{0.97}C_{0.03}$:H passivation layer and a-$Si_{0.50}C_{0.50}$:H mirror layer on both sides.

In an in-situ process an amorphous silicon carbide a-Si_xC_{1-x}:H layer (passivation layer) with ($x \approx 0.97$) was deposited using methane (CH_4), silane (SiH_4) and hydrogen (H_2) as precursor gases at a temperature of 270°C. A second stoichiometric a-SiC:H layer (mirror layer) was deposited in-situ using the same precursors. The samples for lifetime evaluation were processed exactly the same way on both sides (see Fig. 2). The development of this passivation layer stack and the function of the mirror layer are described in detail in our previous work [4].

B. Lifetime measurements

For the determination of τ_{eff}, a µW-PCD tool is used (*WT2000* from the manufacturer *Semilab*). Primarily introduced for measurements with Si material, it is able to measure Ge regardless of its high carrier mobility. The technique is based on laser excitation and measuring the decay of an induced photoconductance. More details can be found in our previous work [4]. The disadvantage of the µW-PCD method is the unknown level of excess carrier density Δn. Therefore, we estimated Δn with the help of the following equation

$$\Delta n = G \cdot \tau_{\text{eff}} \qquad (1)$$

which becomes

$$\Delta n = G \cdot t_{\text{puls}} \qquad (2)$$

for short illumination times t_{puls}. G is the generation rate of election/hole pairs and can be approximated with

$$G = \frac{I_{Laser}}{W \cdot E_{Photon}} (1 - R(\lambda_{\text{Laser}})) \qquad (3)$$

when we assume that all laser light which is not reflected (represented by the reflectivity $R(\lambda_{\text{Laser}})$) is absorbed in the sample with the thickness W and that all absorbed photons with the energy E_{photon} generate exactly one electron/hole pair. In our tool, the maximum laser intensity is $I_{\text{laser}} = 17$ W/m² at a wavelength of $\lambda_{\text{Laser}} = 904$ nm and a pulse duration of $t_{\text{puls}} = 200$ ns. By changing the laser intensity and using Eq. 2 we can conduct an excess carrier density dependent lifetime measurement for all three doping levels (**low**, **medium** and **high**), the results are depicted in Fig. 3. It can be seen that for low Δn the lifetimes show a large experimental error which decreases for increasing Δn. The vertical line at 2×10^{16} at/cm³ indicates the excess carrier density which is normally used for lifetime measurements. To obtain reliable lifetime results, the measurements should be conducted at an excess carrier density where the dependency of lifetime on Δn is low. Such behavior is expected at low Δn for µW-PCD [5]. Low Δn means an excess carrier density which is lower than the doping level of the wafer. According to our estimated Δn, the excess carrier density corresponds to the doping level in the case of lowly doped Ge and the excess carrier density is lower than the doping level for medium and highly doped Ge. Therefore, the requirement for reliable µW-PCD measurements is fulfilled. Nevertheless, for medium and highly doped Ge, the lifetime is depending on Δn in the region of normal laser excitation, while the dependency is less pronounced for the lowly doped samples. This underlines the importance of taking the excess carrier density dependency into account for lifetime measurements.
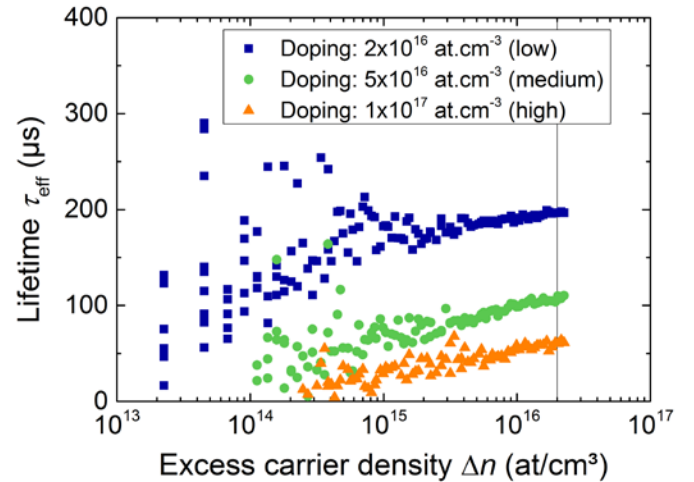

Fig. 3. Injection dependent µW-PCD measurement for all three Ge bulk doping levels.

The Hall measurements for determining μ_{maj} are done with the Van-der-Pauw method [6]. The passivation layer is removed at all four corners and the sample is contacted by Cu tips.

C. Irradiation

1 MeV Electron irradiation (flux of 5×10^{11} e/cm²/s) were performed at *SIRIUS* Irradiation facility (Palaiseau, France) on different lifetime Ge samples with fluences of up to 3×10^{15} e/cm². These electron energy, flux and fluences are typical to the ones used for simulating solar cells degradations under irradiation for space applications. The irradiations were done with several repetitions to get a reliable result. All

irradiated samples were measured before and after irradiation in order to analyze the changes in τ_{eff} as a function of the electron fluence.

D. Simulation

For the potential analysis due to a surface passivation of the backside of the Ge sub-cell, a model for the 3-junction GaInP/GaAs/Ge solar cell was implemented in *Sentaurus Device* [7]. The improvements in V_{OC} and J_{SC} are analyzed for the three doping levels after five different electron fluences. For these sub-cell simulations the two cells above the Ge cell are optically modelled, whereas the Ge sub-cell itself is modelled optically and electrically using measured Ge lifetimes τ_{eff} as an approximation for the bulk lifetime τ_{bulk}. Three different passivation qualities are simulated, which are represented by a surface recombination velocity of $S = 1\times10^7$, 1×10^4 and 10 cm/s (no passivation, imperfect passivation and perfect passivation).

III. RESULTS AND DISCUSSION

In Fig. 4 the decrease of τ_{eff} due to electron irradiation with increasing fluence is depicted for all three Ge doping levels. In general, τ_{eff} is higher for lower doped samples. The lowly doped wafers show $\tau_{eff} > 200\,\mu s$ before irradiation, whereas the highly doped wafers start only with $\tau_{eff} > 50\,\mu s$. This allows for an estimation for an upper limit of S with the help of the following equation [8]

$$\frac{1}{\tau_{eff}} = \frac{1}{\tau_{bulk}} + \frac{2}{W} \times S_{eff} , \qquad (4)$$

where τ_{bulk} is the bulk lifetime and W the wafer thickness. For the upper estimation we set $\tau_{bulk} \to \infty$ and get $S_{max} = 600$ cm/s for the highly doped sample.
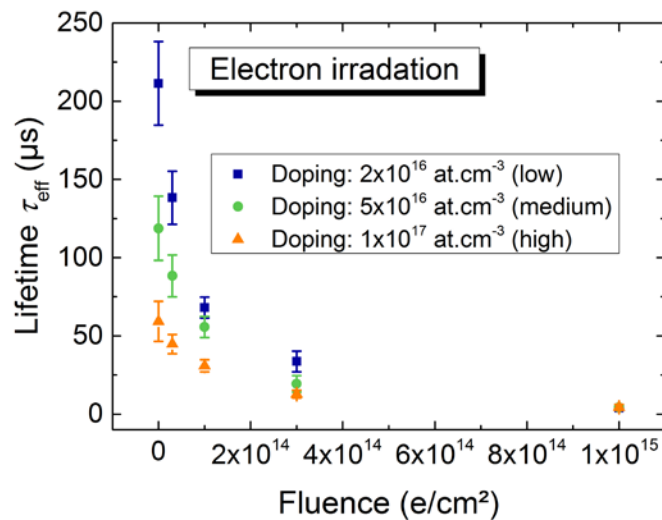

Fig. 4. Lifetime decrease over electron irradiation fluence for all three Ge bulk doping levels.

For all three doping levels, τ_{eff} decreases continuously with increasing electron fluence down to 4 µs after 1×10^{15} e/cm². Every incoming electron introduces a defect in the Ge bulk, which acts as recombination center and results in the decrease of τ_{eff} for increasing fluences.

TABLE I.   LIFETIME VALUES AFTER IRRADIATION WITH VARIOUS ELECTRON FLUENCES USED AS INPUT PARAMETERS FOR THE SIMULATIONS.

fluences (e/cm²)	Minority carrier lifetime τ_{eff} (µs)		
	Low dop.	Medium dop.	High dop.
0 (BOL)	206	118	54
1×10^{14}	72	56	29
3×10^{14}	34	19	12
1×10^{15} (EOL)	4	4	4

In Tab. I, selected measured τ_{eff} from Fig. 3 are listed. Another material property, which could be changed through electron irradiation is the minority carrier mobility μ_{min}. As it is difficult to access μ_{min} experimentally, we assume that a change in μ_{min} should correlate with a change in μ_{maj}. The latter can be determined by Hall measurements. The results for all three doping levels before and after irradiation are listed in Tab. II together with literature values.

TABLE II.   MEASURED MAJORITY CARRIER MOBILITY BEFORE AND AFTER ELECTRON IRRADIATION FOR ALL THREE GE BULK DOPING LEVELS AND LITERATURE VALUES BEFORE IRRADIATION FOR COMPARISON.

Doping (at/cm³)	Majority carrier mobility Ge wafer (cm²/Vs)		
	Before irr.	After irr.	Literature [9]
1.0×10^{17}	1220 ± 90	1250 ± 30	996 ± 30
5.0×10^{16}	1440 ± 50	1440 ± 100	1206 ± 30
2.3×10^{16}	1790 ± 40	1740 ± 140	1425 ± 20

Within the accuracy of the measurement, no change of μ_{maj} due to electron irradiation is detected. Furthermore, the experimental values for μ_{maj} are higher than the literature values. This is attributed to the very high quality of the Ge wafers used in this experiment. We conclude from µW-PCD and Hall measurements that electron irradiations influence the lifetime whereas the mobility is not affected.

The data from Tab. I is used as input for the solar cell simulations. Former experiments and simulations have shown that IV parameters, EQE, etc. of simulated and measured 3-junction cells are in good agreement before and after electron irradiation if no surface passivation ($S = 10^7$ cm/s) at the Ge backside is assumed [10].

In our study, the IV characteristic of the Ge sub-cell was modelled in dependency of S at the backside contact. The results for Ge sub-cells with begin of life (BOL) lifetime are shown in Fig. 5 for a doping concentration of 10^{17} at/cm³ for three different thicknesses. A gain of almost 1 mA/cm² in J_{SC}

and ≈ 50 mV in V_{OC} can be achieved due to surface passivation. For thin cells (40 µm) the V_{OC} improvement is most pronounced and leads to an additional gain between $S = 10^4$ and 1 cm/s.
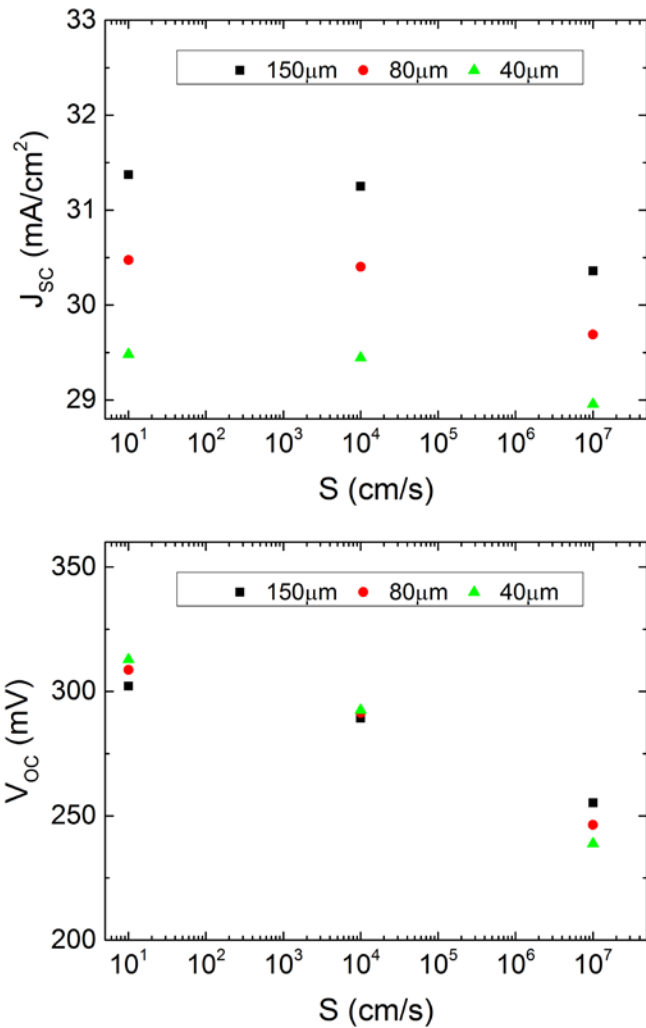
electron fluences below 1×10^{15} e/cm². One can also see that low doping should be favored for good backside passivation and low electron fluences, whereas high doping gives the best results after high electron fluences.
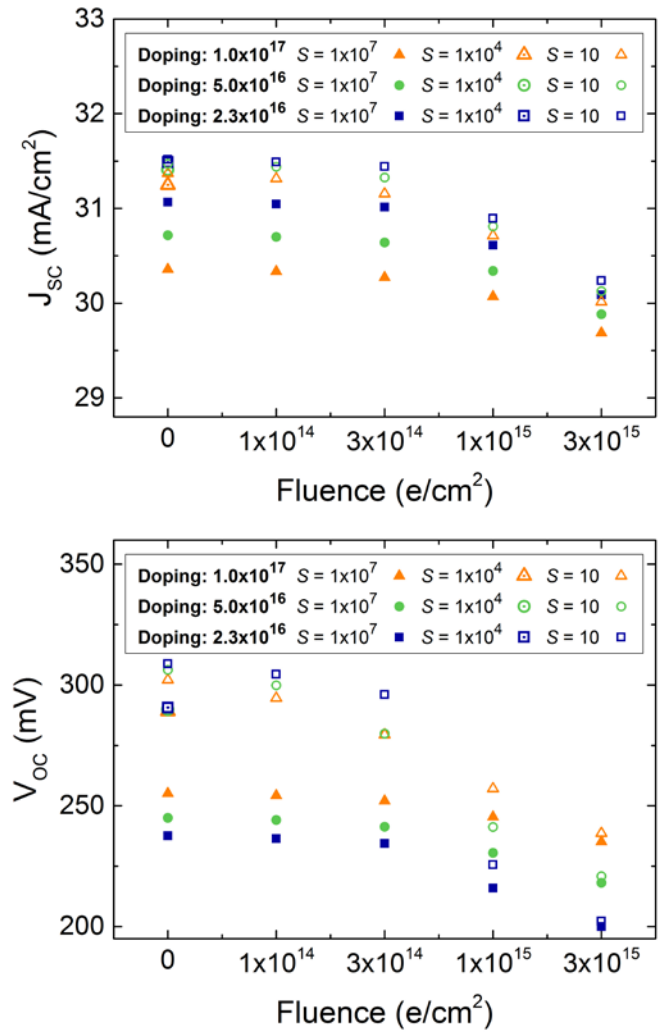

Fig. 5. Simulated dependencies of short circuit current J_{SC} (top) and voltage V_{OC} (bottom) of the Ge sub-cell on the surface recombination velocity S for a Ge bulk dopant concentration of 10^{17} at/cm³ for three different thicknesses.

Fig. 6. Simulated dependencies of sub-cell J_{SC} (top) and V_{OC} (bottom) on the electron fluence for a Ge cell thickness of 150 µm and varying S (in cm/s) and dopant concentrations (in at/cm³).

However, the simulation shows that even for an imperfect surface passivation with $S = 10^4$ cm/s a strong improvement of J_{SC} and V_{OC} can be achieved independent of the thicknesses. In a next step, we analyze how much the J_{SC} and V_{OC} gain due to passivation diminishes for lower lifetime after electron irradiation in comparison to BOL. Fig. 6 shows the J_{SC} and V_{OC} for 150 µm thick Ge cells in dependency of the electron fluences for different doping concentrations and S.

As expected, the improvement due to surface passivation is lost for degraded cells with a strong lifetime limitation by irradiation damage. However, for moderate doping significant improvements can be achieved with surface passivation for

Furthermore, the simulation shows that even for an imperfect surface passivation with S of 10^4 cm/s (symbols with dot in the center, only calculated for BOL) a strong improvement of J_{SC} and V_{OC} can be achieved. This is especially encouraging, as our upper estimate for S (600 cm/s) is well below the simulated imperfect passivation.

In summary, backside passivation is a promising step to increase significantly J_{SC} and V_{OC} of Ge sub-cells which underwent electron fluences not higher than 3×10^{14} e/cm². For higher electron fluences τ_{eff} is limited by irradiation damage and the gain diminishes.

However, for the industrial relevant 3-junction solar cell concepts the current is limited by the top cell. Thus, the J_{SC}

gain in the Ge sub-cell has only small influence on the overall J_{SC} of the triple junction. This completely changes when assuming 4-junction solar cells. There the current generation in the indirect regime of the Ge bottom solar cell defines the overall achievable current. A gain in current there leads directly to a significant increase in efficiency of the device. 4-junction solar cells based on Germanium allow for currents between 11 and 13 mA/cm². An increase of 0.8 - 1.7 mA/cm² in the Ge bottom solar cell can lead to current increases of 0.2 - 0.4 mA/cm² in the device, which is a 2 - 4% increase in current and thus a similar relative increase in efficiency. In Fig. 7 the simulation of the absorption of a 4-junction solar cell is depicted for the standard case (dotted lines) and the improved Ge back side (solid lines). The improvement of the Ge cell (blue lines) in the long wavelength range is clearly visible. To make use of this current gain, the top solar cell band gaps have to be slightly shifted to lower band gaps, which on the other hand leads to a voltage decrease that slightly decreases the possible efficiency gain.
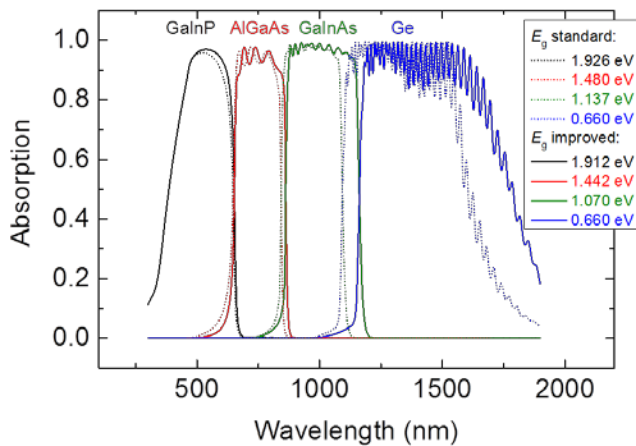

Fig. 7.   Simulation of 4-junction solar cell with (solid lines) and without (dotted lines) improved back side. The improvement of the overall cell performance is due to the enhanced absorption in the infrared wavelength range, which leads to higher currents.

Estimations for a 4-junction solar cell predict up to 1% absolute gain in BOL efficiency, when implementing the rear-side passivation.

CONCLUSION

An efficient rear-side passivation based on a-Si$_x$C$_{1-x}$:H layers for multi-junction space solar cells based on Ge substrates is presented. This surface passivation procedure leads to minority carrier lifetimes $\tau_{eff} \approx 200\,\mu$s. Electron irradiation for accelerated aging of passivated Ge samples leads to a significant minority carrier lifetime decrease whereas the majority carrier mobility stays constant. These findings allow for simulations of the potential of the rear-side passivation on the Ge sub-cell in multi-junction concepts. An important result is that even an imperfect passivation ($S = 10^4$ cm/s) results in

quite similar gains compared to a perfect passivation ($S = 10$ cm/s), which is a significant increase in J_{SC} (≈ 1 mA/cm^2) and V_{OC} (≈ 60 mV) of the Ge sub-cell. This improvement can increase the efficiency of 4-junction solar cells up to 1%. Another effect which will increase efficiency, the advanced reflection at the cell's rear-side which will lead to lower cell temperatures and therewith to higher V_{OC}, has not been taken into account yet. The fabrication of multi-junction solar cells with the new a-Si$_x$C$_{1-x}$:H / a-SiC:H rear-side layer stack is ongoing.

REFERENCES

[1]   Carsten Baur, "Pathways to Next Generation Space Solar Cells," Kitakyushu, Oct. 29 2009.

[2]   J. Fernandez, S. Janz, D. Suwito, E. Oliva, and F. Dimroth, "Advanced concepts for high-efficiency Ge photovoltaic cells," in *33rd IEEE Photovoltaic Specialist Conference: Proceedings*, San Diego, CA, USA, 2008.

[3]   J. Fernández *et al.*, "Back-surface Optimization of Germanium TPV Cells," *AIP Conference Proceedings*, vol. 890, no. 1, pp. 190–197, 2007.

[4]   S. Janz *et al.,* "Amorphous silicon carbide rear-side passivation and reflector layer stacks for multi-junction space solar cells based on germanium substrates," in *44th IEEE Photovoltaic Specialist Conference: Proceedings*, Washington, DC, 2017, to be published.

[5]   D. Walter *et al.,* "Determining the minority carrier lifetime in epitaxial Si layers by µW-PCD measurements," in *25th European Photovoltaic Solar Energy Conference*, Valencia, Spain, 2010, pp. 2078–2083.

[6]   L. J. van der Pauw, "A method of measuring specific resistivity and Hall coefficient of lamellae of arbitrary shape," *Philips Technical Review*, vol. 13, no. 8, pp. 220–224, 1958/1959.

[7]   Synopsys, SentaurusTM User Guide, release I-2013.12.

[8]   S. W. Glunz, "Ladungsträgerrekombination in Silicium und Siliciumsolarzellen," Dissertation, Albert-Ludwigs-Universität, Freiburg, 1995.

[9]   P. H. Nguyen, K. R. Hofmann, and G. Paasch, "Comparative full-band Monte Carlo study of Si and Ge with screened pseudopotential-based phonon scattering rates," *Journal of Applied Physics*, vol. 94, no. 1, pp. 375–386, 2003.

[10] S. P. Philipps *et al.,* "III-V Multi-Junction Solar Cells - Simulation and Experimental Realizaton," *Informacije MIDEM - Journal of Microelectronics, Electronic Components and Materials*, no. 39, pp. 201–208, 2009.